Scalable Multiuser Immersive Communications with Multi-numerology and Mini-slot

Ming Hu, Jiazhi Peng, Lifeng Wang, and Kai-Kit Wong

***Abstract*—This paper studies multiuser immersive communications networks in which different user equipment may demand various extended reality (XR) services. In such heterogeneous networks, time-frequency resource allocation needs to be more adaptive since XR services are usually multi-modal and latency-sensitive. To this end, we develop a scalable time-frequency resource allocation method based on multi-numerology and mini-slot. To appropriately determining the discrete parameters of multi-numerology and mini-slot for multiuser immersive communications, the proposed method first presents a novel flexible time-frequency resource block configuration, then it leverages the deep reinforcement learning to maximize the total quality-of-experience (QoE) under different users' QoE constraints. The results confirm the efficiency and scalability of the proposed time-frequency resource allocation method.**

***Index Terms*—Immersive communications, quality of experience, numerology, mini-slot.**

I. Introduction

The sixth-generation wireless (6G) communications systems seek to boost scalable and resilient transmissions for addressing new challenges, which come from the emerging multi-modal extended reality (XR) services. As one of 6G key use cases, immersive communications provide remote XR services including mixed reality and augmented reality, however, these immmersive services impose stringent requirements on data rate and communications latency [1, 2]. Multi-numerology and mini-slot are compelling access technologies for supporting diverse scenarios and requirements, which have been applied in 5G systems [3].

Since sub-6 GHz, millimeter wave (mmWave) and terahertz (THz) frequency bands shall be widely-used in 6G, the frequency bandwidths at different carrier frequencies are dramatic, which may substantially increase system complexity and peak-to-average power ratio (PAPR) if the number of subcarriers increases with adding more frequency bandwidths. In light of hardware constraints and various XR service requirements, multi-numerology is introduced to make flexible resource allocation, compared to the uniformly distributing frequency resource allocation in 5G systems [4]. Its gist is that subcarrier spacing can be tuned according to the specific frequency bandwidths and service requirements, in this way, the number of subcarriers can keep the same for different amounts of frequency bandwidths without largely increasing the PAPR. To meet the requirements of mission-critical services, [5] proposes a scalable resource block based on flexible numerology. In [6], mixed-numerology is adopted in windowed orthogonal frequency division multiplexing (OFDM) systems. Like traditional single-numerology case, multi-numerology OFDM systems are still susceptible to the critical PAPR, hence [7] proposes a numerology scheduling method to reduce the PAPR. The numerology scheduler of [8] is designed to be adaptive for satisfying different slices' requirements. In vehicle-to-everything networks, recent work [9] shows that the use of 5G numerology can improve Quality-of-Service. On the other hand, mini-slot is an alternative for further enhancing the network's scalability, which achieves much lower latency since it allows shorter transmission slot duration to contain only a few OFDM symbols, therefore, mini-slot plays a promising role in ultra-reliable low-latency communication (URLLC). When URLLC and the enhanced mobile broadband (eMBB) traffics coexist in multiuser communications systems, [10] provides a media access control layer scheduling for maximizing eMBB utility under URLLC latency constraint. To flexibly manage the eMBB and URLLC network slices, [11] investigates the numerology and mini-slot for maximizing the network throughput while satisfying service level agreement. Meanwhile, [12] develops a hybrid puncturing and superposition scheme which can maximize the minimum average throughput of eMBB and URLLC users. The work of [13] aims to maximize the minimum achievable transmission rate through optimizing the multi-numerology and mini-slot.

In immersive communications systems, 360° video is an important component for XR applications [2, 14]. However, 360° video streaming demands large frequency bandwidths for low-latency transmissions. Existing research contributions have attempted to improve the efficiency of 360° video streaming under limited resources constraints. In [15], a two-tier 360-degree video streaming scheme is investigated to address the network dynamics, such a scheme is source representation independent and outperforms the DASH streaming and Field of View (FoV) streaming schemes. Since videos in the FoV region must be delivered, [16] analyzes the future FoV region in a closed-form under a given confidence level. By considering the tile-based 360-degree video streaming, [17] adopts a machine learning method to optimize different Quality of Experience (QoE) objectives. A viewport-aware adaptive tiling scheme is studied in [18], where the long-term user QoE is maximized. In [19], energy efficiency of delivering

Manuscript received September 16, 2023; revised November 28, 2023 and January 09, 2024; accepted February 25, 2024. This work was supported in part by the National Key Research and Development Program under Grant 2021YFE0193300, and in part by Shanghai STCSM Program under Grant 22511100802. The associate editor coordinating the review of this article and approving it for publication was C. Tsinos. *(Corresponding author: Lifeng Wang.)*

M. Hu, J. Peng, and L. Wang are with the School of Information Science and Engineering, Fudan University, Shanghai 200433, China (e-mail: 20210720045, 21210720209, lifengwang@fudan.edu.cn).

K.-K. Wong is with the Department of Electronic and Electrical Engineering, University College London, London WC1E 7JE, U.K. (e-mail: kai-kit.wong@ucl.ac.uk).

multi-quality tiled 360 virtual reality videos is enhanced by jointly determining appropriate beamforming, subcarrier and the choices of quality level. Latest work [2] designs flexible frame structures for achieving the two-tier 360-degree video delivery and improving the system robustness.

Motivated by the aforementioned studies, this paper aims to establish the scalable two-tier 360-degree video streaming in multiuser immersive communications systems by leveraging multi-numerology and mini-slot according to the 3GPP [3, 13, 20]. To the best of our knowledge, this is the first work to exploit the merits of joint multi-numerology and mini-slot design for 360-degree video delivery. We orchestrate a flexible time-frequency resource block structure and propose a novel time-frequency allocation method to maximize the total QoE under diverse levels of UE's QoE constraint, which significantly outperforms the QoE-based greedy and equal resource allocation solutions.

II. System Descriptions

In a downlink immersive communications system, base station (BS) delivers 360-degree video contents to N user equipment (UEs). To meet different UEs' QoE, we manage time-frequency resources via numerology and mini-slot. According to the 5G new radio (5G NR) [3, 13, 20], each subframe duration is fixed value of 1ms, the OFDM's subcarrier spacing is $15 \times 2^{\mu}$kHz with the numerology μ (a non-negative integer value for low-latency XR services), and each resource block has 12 consecutive subcarriers with the same numerology in the frequency domain. Note that each slot contains 14 OFDM symbols, and 4G LTE's numerology is $\mu = 0$ with the slot duration of 1ms [3]. For generality, we consider that the n-th UE's mini-slot duration can be selected to contain η_n OFDM symbols, and each slot is divided into several mini-slots whose lengths may be different. As such, we design a new time-frequency resource block configuration (the unit is ms×kHz=s×Hz) to achieve scalable multiuser immersive communications, which is defined as follows:

$$\begin{aligned} \mathrm{C}^{\mathrm{RB}} &= \Delta T_{\min} \times \Delta B_{\min} \\ &= \frac{1}{14 \times 2^{\mu_{\max}}} \times \left(12 \times 15 \times 2^{\mu_{\min}}\right), \end{aligned} \tag{1}$$

where $\Delta T_{\min} = \frac{1}{14 \times 2^{\mu_{\max}}}$ms is the minimum OFDM symbol duration that can be supported in the system with the maximum numerology value $\mu_{\max}$, considering the fact that the OFDM symbol duration without cyclic prefix (CP) changes inversely to its subcarrier spacing; $\Delta B_{\min} = 12 \times 15 \times 2^{\mu_{\min}}$kHz is the minimum bandwidth part in the frequency domain with the minimum numerology value $\mu_{\min}$, here, the bandwidth part is a subset of resource blocks for a given numerology [20]. The advantage of such a resource block design is that it solely depends on the system's maximum and minimum numerology values regardless of UEs' specific XR service requirements, in this case, the size of a bandwidth part (the unit is ms×kHz=s×Hz) occupied by the n-th UE with the required numerology μ_n and mini-slot η_n can be easily calculated as

$$\begin{aligned} \mathrm{C}^{\mathrm{BWP}} &= \left(\eta_n \times 2^{\mu_{\max}-\mu_n} \Delta T_{\min}\right) \times \left(2^{\mu_n - \mu_{\min}} \Delta B_{\min}\right) \\ &= \eta_n \times 2^{\mu_{\max}-\mu_{\min}} \times \mathrm{C}^{\mathrm{RB}}. \end{aligned} \tag{2}$$

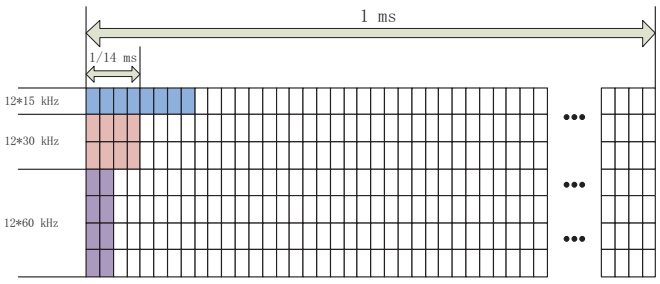

Fig. 1. An illustration of time-frequency resource structure with multi-numerology ($\mu \in \{0, 1, 2\}$ in this figure) and the same mini-slot value $\eta = 2$ for all the UEs, in which each rectangle of the resource grid represents a resource block given by (1), and each UE's allocated bandwidth part has the same number of resource blocks given by $\mathrm{C}^{\mathrm{BWP}} = 8\mathrm{C}^{\mathrm{RB}}$ according to (2), regardless of each UE's numerology.

Each bandwidth part is dedicated to one UE and there is no overlap between them. From (2), the number of resource blocks in each UE's allocated bandwidth part only depends on its mini-slot for a given immersive communications system, as illustrated in Fig. 1.

In the two-tier 360-degree video streaming system [2], each video frame has the duration of T (ms) and frequency bandwidth B (kHz), which is partitioned into basic tier (BT) video chunk phase and and enhancement tier (ET) video chunk phase [15]. Let μ_n^{BT}, η_n^{BT}, μ_n^{ET}, and η_n^{ET} denote the BT's and ET's numerology and mini-slot, respectively. Based on (2), we have the following time resource constraint

$$\begin{aligned} &\sum_{\substack{(i,i')\in\{\mathcal{L},\mathcal{R}\},\\(i,i')\notin\{\mathcal{B},\mathcal{A}\}}} \eta_{n,i}^{\mathrm{BT}} 2^{\mu_{\max}-\mu_{n,i}^{\mathrm{BT}}} \Delta T_{\min} + \\ &\sum_{\substack{(j,j')\in\{\mathcal{L},\mathcal{R}\},\\(j,j')\notin\{\mathcal{B},\mathcal{A}\}}} \eta_{n,j}^{\mathrm{ET}} 2^{\mu_{\max}-\mu_{n,j}^{\mathrm{ET}}} \Delta T_{\min} \le T, \quad \forall n, \end{aligned} \tag{3}$$

and frequency resource constraint

$$\sum_{\substack{(i,i')\in\{\mathcal{B},\mathcal{A}\},\\(i,i')\notin\{\mathcal{L},\mathcal{R}\}}} 2^{\mu_{n,i}^{\nu}-\mu_{\min}} \Delta B_{\min} \le B, \quad \forall n, \nu \in \{\mathrm{BT}, \mathrm{ET}\}, \tag{4}$$

where $\mu_{n,i}^{\mathrm{BT}}$ and $\eta_{n,i}^{\mathrm{BT}}$ are the numerology and mini-slot of the i-th bandwidth part at BT for the UE n, respectively, $\mu_{n,j}^{\mathrm{ET}}$ and $\eta_{n,j}^{\mathrm{ET}}$ are the numerology and mini-slot of the j-th bandwidth part at ET for the UE n, respectively, the relative positioning constraint $(i, i') \in \{\mathcal{L}, \mathcal{R}\}$ means that the bandwidth part i is the left or right of the bandwidth part i', i.e., there is no overlap between them in the time domain, the relative positioning constraint $(i, i') \in \{\mathcal{B}, \mathcal{A}\}$ means that the bandwidth part i is the below or above of bandwidth part i', i.e., there is no overlap between them in the frequency domain,

Since the time-frequency resources are orthogonally allocated to the UEs (no co-channel interference), the BT's transmission rate (bits per frame) is given by

$$R_n^{\mathrm{BT}} = \sum_i \mathrm{C}_{\mathrm{BT},n,i}^{\mathrm{BWP}} \log_2 \left(1 + \frac{G_n^{\mathrm{t}} G_n^{\mathrm{r}} \left|\hbar_n^{\mathrm{BT}}\right|^2 p_n}{\delta^2}\right), \tag{5}$$

where $\mathrm{C}_{\mathrm{BT},n,i}^{\mathrm{BWP}}$ is the i-th bandwidth part allocated to the n-th UE at BT with the mini-slot $\eta_{n,i}^{\mathrm{BT}}$, G_n^{t} and G_n^{r} are the effective

transmit antenna gain and receive antenna gain obtained by the UE n, respectively, $\left|\hbar_n^{\mathrm{BT}}\right|^2$ and $\left|\hbar_n^{\mathrm{ET}}\right|^2$ are the large-scale fading channel power gains[1] p_n is the transmit power spectral density (PSD) of the downlink channel between the BS and the n-th UE, and δ^2 is the noise's PSD. Likewise, ET's transmission rate (bits per frame) is given by

$$R_n^{\mathrm{ET}} = \sum_j \mathrm{C}_{\mathrm{ET},n,j}^{\mathrm{BWP}} \log_2 \left(1 + \frac{G_n^{\mathrm{t}} G_n^{\mathrm{r}} \left|\hbar_n^{\mathrm{ET}}\right|^2 p_n}{\delta^2}\right), \tag{6}$$

where $\mathrm{C}_{\mathrm{ET},n,j}^{\mathrm{BWP}}$ is the j-th bandwidth part allocated to the n-th UE at ET with the mini-slot $\eta_{n,j}^{\mathrm{ET}}$. We further highlight that the proposed resource block and bandwidth part designs facilitate the analysis of transmission rate in multiuser communications since (5) and (6) are available for arbitrary UEs' numerologies.

One of the key performance indicators (KPIs) in the two-tier video delivery system is the QoE, which is commonly-measured in a logarithmic manner [15, 18], i.e., the QoE for the n-th UE is calculated as

$$\widetilde{Q}_n = (1-\rho_n)\, Q_n\left(\hat{R}_n^{\mathrm{BT}}\right) + \rho_n Q_n\left(\Xi_n\right), \tag{7}$$

where ρ_n $(0 \le \rho_n \le 1)$ is the probability of precisely predicting UE's FoV, $Q_n(x) = a_n + b_n \log(x)$ with specific XR video-dependent constant parameters a_n and b_n, $\hat{R}_n^{\mathrm{BT}} = \frac{R_n^{\mathrm{BT}}}{\mathcal{C}^{\mathrm{BT}}}$ with the coverage area of the 360° video $\mathcal{C}^{\mathrm{BT}}$, $\Xi_n = \hat{R}_n^{\mathrm{BT}} + \hat{R}_n^{\mathrm{ET}}$ denotes the effective rate after using layered coding to generate the ET chunks, here $\hat{R}_n^{\mathrm{ET}} = \frac{R_n^{\mathrm{ET}}}{\mathcal{C}^{\mathrm{ET}}}$ with the coverage area of the ET chunk $\mathcal{C}^{\mathrm{ET}}$.

By appropriately selecting numerology and mini-slot, our aim is to maximize the total QoE while achieving the minimum QoE per active UE, thus the time-frequency resource allocation problem is formulated as

$$\begin{aligned}
&\max_{\mathbf{x},\boldsymbol{\mu},\boldsymbol{\eta}} \sum_{n=1}^{N} x_n \widetilde{Q}_n \qquad (8)\\
&\text{s.t. } \mathrm{C1}: x_n \in \{0,1\}, x_n\left(Q_n\left(\hat{R}_n^{\mathrm{BT}}\right) - \overline{Q}_n^{\min}\right) \ge 0, \quad \forall n,\\
&\quad \mathrm{C2}: Q_n\left(\hat{R}_n^{\mathrm{BT}}\right) \le \gamma_n^{\mathrm{peak}} \overline{Q}_n^{\min}, \quad \forall n,\\
&\quad \mathrm{C3}: \mathrm{Eq.(3)},\ \ \mathrm{Eq.(4)},\\
&\quad \mathrm{C4}: \mathrm{C}_{\nu,n,i}^{\mathrm{BWP}} \bigcap \mathrm{C}_{\nu',n',i'}^{\mathrm{BWP}} = \emptyset, \quad \forall n,\nu,\nu' \in \{\mathrm{BT},\mathrm{ET}\},\\
&\quad \mathrm{C5}: \mu_{n,i}^{\nu} \in \mathbb{Z}, \eta_{n,i}^{\nu} \in \mathbb{Z}, \eta_{n,i}^{\nu} \le 14, \quad \forall n,\nu, \in \{\mathrm{BT},\mathrm{ET}\},
\end{aligned}$$

where $\mathbf{x} = [x_n]$ are binary values that indicate whether UE is served or not, $\boldsymbol{\mu} = [\mu_{n,i}^{\mathrm{BT}}, \mu_{n,i}^{\mathrm{ET}}]$ and $\boldsymbol{\eta} = [\eta_{n,i}^{\mathrm{BT}}, \eta_{n,i}^{\mathrm{ET}}]$. Constraint C1 makes sure the served UEs meet the minimum QoE value $\overline{Q}_n^{\min}$ and the solutions of problem (8) are always feasible; C2 shows that the QoE for entire 360° view at BT needs to be restricted to below a peak value $\gamma_n^{\mathrm{peak}} \overline{Q}_n^{\min}$ in practice, since QoE for viewport videos at ET is more important; C3 is the limitation of available time-frequency resources; C4 illustrates that there is no overlap among bandwidth parts; In constraint C5, mini-slot $\eta_{n,i}^{\nu} \le 14$ means that each slot consists of several mini-slots and there are always 14 OFDM symbols per slot regardless of the specific numerology [3, 13].

[1]In the highly directional beamforming transmissions such as millimeter wave (mmWave), the effect of small-scale fading on the channel power gain could be ignored.

III. DRL-based Algorithm Design

Problem (8) is combinatorial with non-overlap constraints, which is challenging to solve. Since deep reinforcement learning (DRL) is a powerful machine learning tool to deal with discrete decision-making problems, we provide a DRL-based solution, in which an agent (link between the UE and BS) interacts with its environment, and the key components of RL are detailed as follows:

- State: In a given resource grid with time and frequency boundaries, the observed state space at BS is denoted by $\mathcal{S} = \{\boldsymbol{\Theta}, \boldsymbol{\Psi}, \boldsymbol{\aleph}, \boldsymbol{\Phi}\}$, where $\boldsymbol{\Theta}$ contains the allocated bandwidth parts and idle ones, $\boldsymbol{\Psi}$ contains the allocated BT and ET's bandwidth parts for each UE and the corresponding QoE $Q\left(\hat{R}^{\mathrm{BT}}\right)$ and $\widetilde{Q}$ given by (7), $\aleph$ contains the order of serving UE at each time-step, and Φ contains the time and frequency boundary lines of the allocated resources at the beginning of each episode. The state vector at each time-step is $\mathbf{s}_t \in \mathcal{S}$.
- Actions: The action a_t taken by the agent include the numerology μ, mini-slot η and their corresponding bandwidth part $\mathrm{C}^{\mathrm{BWP}}$ given by (2) (as illustrated Fig. 1). Given the state $\mathbf{s}_t$, agent chooses feasible numerology and mini-slot values based on constraints C1 and C5 (Note that both the objective and constraint C1 of problem (8) only depend on the selected mini-slot thanks to our resource block and bandwidth part designs in Section II.), and thus determines feasible bandwidth parts based on the current time and frequency boundary lines, to satisfy the constraints C3-C4.
- Reward: When the action is executed, agent obtains a reward. Let M denote the maximum allowable number of time-steps before terminating an episode, and the reward function is given by

$$r_{n,t} = \begin{cases} \varrho \Delta\widetilde{Q}_n(t) + (1-\varrho)\,\mathcal{Z}, \text{ if C1} - \text{C5 are met,} \\ \mathcal{H}, \text{ if episode terminates and C1} - \text{C5 are met,} \\ \Theta, \text{ otherwise,} \end{cases}$$

where $\Delta\widetilde{Q}_n(t) = \widetilde{Q}_n(t) - \widetilde{Q}_n(t-1)$ is the incremental value of the agent's QoE at time-step t, $\mathcal{Z}$ is a penalty to enable that the agent is time-aware (namely limited number of time-steps for the agent's interaction with the environment) [8, 21], which is much helpful for system stability and low-latency immmersive communications, ϱ is the weighting parameter, a high reward value $\mathcal{H}$ is obtained if the episode terminates and constraints C1-C5 are met, otherwise incurring a penalty Θ.

In light of deep Q-learning [22], we propose a DRL-based algorithm to solve the problem (8), which is detailed in **Algorithm 1** at next page. The deep Q-network of **Algorithm 1** is illustrated in Fig. 2.

IV. Simulation Results

This section provides numerical results to confirm the efficiency of the proposed DRL-based time-frequency resource allocation in Section III. The learning parameters include:

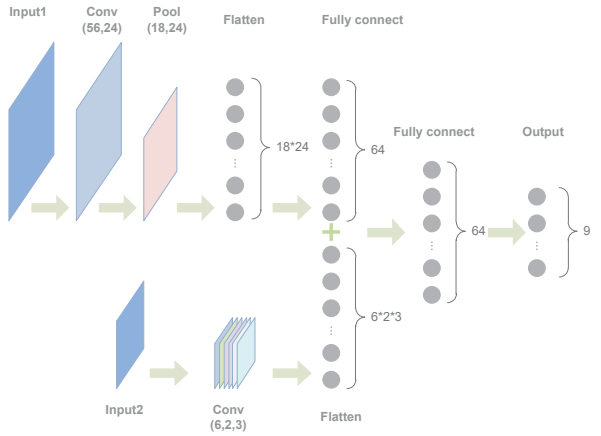

Fig. 2. Deep convolutional neural network structure in the proposed DQN-based method.

Algorithm 1: DRL based Time-frequency Resource Allocation

Initialize the maximum number of episodes E, the maximum allowable number of time-steps M per episode, and deep Q-network (shown in Fig. 2); the episode index $e = 1$
while $e \leq E$ **do**
  initialize the state space $\mathcal{S}$, in which $\aleph$ is initialized by sorting the UEs in descending order of their QoE levels under equal resource allocation;
  for $t = 1, \cdots, M$ **do**
    a) Select a random action $a_{n,t}$ according to ε-greedy policy. Note that some actions need to be excluded when the constraints C1-C5 are not met;
    b) After executing the selected action, obtain a reward and observe the next state $\mathbf{s}_{t+1}$;
    if constraint C2 is violated **then**
      the corresponding link is no longer considered as an agent at BT phase in this episode;
    end
    c) Store the transitions $\{\mathbf{s}_t, \mathbf{a}_t, \mathbf{r}_t, \mathbf{s}_{t+1}\}$ into memory;
    d) Train the deep Q-network using minibatch of transitions data from the memory;
    e) Update the policy π: $\mathcal{S} \rightarrow \mathbf{a}$;
  end
  iii) $e = e + 1$;
end
The corresponding action $\mathbf{a}$ is obtained

learning rate is 0.001, the maximum allowable number of time-steps per episode is $M = 1000$, the parameters in the reward function are set as $\varrho = 0.5$, $\mathcal{Z} = -0.01$, $\mathcal{H} = 500$, and $\Theta = -2$, respectively, the discount factor $\gamma = 0.99$, and deep Q-network in Fig. 2 are trained using Adam optimizer. The system parameters are detailed in Table I. In the simulations, the communication distance $d_n \geq 1$ from the BS to the n-th UE is uniformly distributed with the cell radius 200m, the probability of precisely predicting UE's FoV ρ_n follows the truncated normal distribution with the truncation interval [0.6,1] (its mean and variance of the parent general normal probability density function are 0.8 and 0.49, respectively), and $a_n = 0$, $b_n = 1$, $\forall n$. The results are obtained by averaging over 2000 trials.

A. Convergence

Fig. 3 confirms that the proposed DRL-based method converges at a fast speed. Moreover, the input dimensionality is not large based on our resource block design given by (1) (56×24 resource blocks in the simulations), which relieves the burden of computation and memory. The maximum average award becomes stable when the number of episodes is greater than $E = 310$.

TABLE I
SIMULATION PARAMETERS

BT view coverage	$\mathcal{C}^{\mathrm{BT}} = 360^\circ \times 180^\circ$
ET view coverage	$\mathcal{C}^{\mathrm{ET}} = 135^\circ \times 135^\circ$
mmWave carrier frequency	$f_c = 28$GHz
System bandwidth	$B = 69.12$MHz
Each video frame duration	$T = 0.0625$ms
Effective transmit antenna gain per UE video	$G_{\mathrm{t}} = 15$dBi
Effective receive antenna gain per UE video	$G_{\mathrm{r}} = 10$dBi
Large-scale channel fading power gain	$\lvert\hbar_n\rvert^2 = \left(\frac{3\times10^8}{4\pi f_c}\right)^2 \times d_n^{-2}$
Noise's PSD	$\delta^2 = -169$dBm/Hz
Total transmit PSD	$p_{\mathrm{total}} = -47$dBm/Hz
Vector of four UEs' minimum QoE levels	$\overline{\mathbf{Q}}_{1\times4} = [4.9, 4.6, 4.8, 4, 6]$
Peak levels of four UEs' QoE at BT	$5\overline{\mathbf{Q}}_{1\times4}$ with $\gamma_n^{\mathrm{peak}} = 5$
Numerology	$\mu = \{4, 5, 6\}$ [13]
Mini-slot	$\eta = \{2, 4, 7\}$ [13]

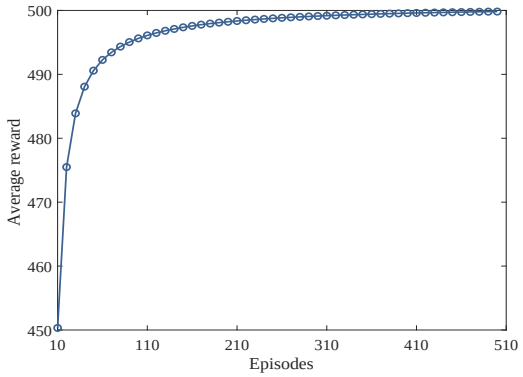

Fig. 3. The convergence of the proposed DRL-based method.

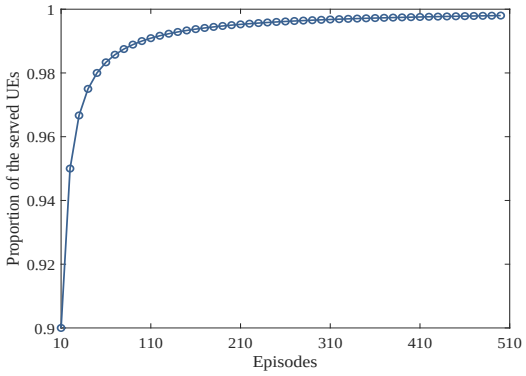

Fig. 4. The feasibility of the proposed DRL-based method.

B. Feasibility

Fig. 4 confirms that the proposed method achieves the feasibility and satisfies the constraints C1-C5 of problem (8), namely the minimum QoE of the served UEs are guaranteed, and the percentage of the served UEs is almost 100% as the number of episodes is larger than 310.

This article has been accepted for publication in IEEE Communications Letters. This is the author's version which has not been fully edited and content may change prior to final publication. Citation information: DOI 10.1109/LCOMM.2024.3370915

C. Efficiency

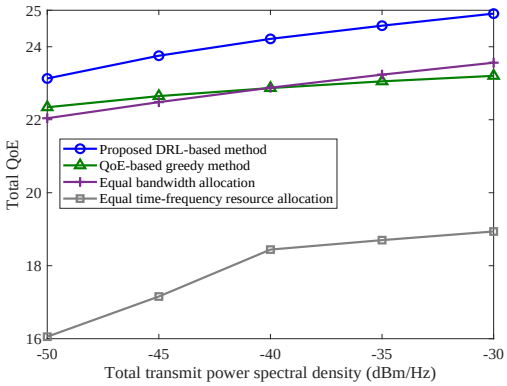

Fig. 5. The performance of the proposed DRL-based method.

Fig. 5 confirms the efficiency of the proposed method compared to the equal resource allocation cases. In the simulations, the number of episodes is set as $E = 510$ based on the empirical results in Figs. 3 and 4. There is no commonly-accepted method yet in this uncharted study and three benchmark solutions are considered as follows: 1) the QoE-based greedy method follows the approach of 3GPP, which allows UEs with higher QoE levels to take priority for resource allocation [23]; 2) the equal bandwidth allocation case considers free-viewpoint without FoV predication [2] (BS sends the entire 360-degree videos to the UEs.); and 3) the equal time-frequency resource allocation case considers that the frequency bandwidths are equally allocated to the UEs and time of each UE's BT is the half of a video frame duration. We see that the proposed DRL-based method outperforms all the benchmark cases. The QoE-based greedy method has better performance than other benchmark cases in the low transmit PSD regime, however, it achieves lower QoE than the equal bandwidth allocation case at higher transmit PSDs since the multiuser diversity gain of the equal bandwidth allocation case is higher than the QoE-based greedy one. In addition, the equal time-frequency resource allocation case obtains the worst QoE performance, due to the fact that in the equal time-frequency resource allocation case, the minimum QoE of some UEs cannot be met when time resources are not enough for BT transmissions, i.e., less UEs are served in this case.

V. Conclusions

In multiuser immersive communications, diverse service requirements posed a great challenge to the time-frequency resource management. To address this issue, the scalable delivery of 360-degree video was considered. By exploiting the numerology and mini-slot techniques, a flexible resource block structure has been designed, which only depends on the system's maximum and minimum numerology. A DRL-based method was developed to optimize the numerology and mini-slot values for maximizing the network QoE. The results confirmed the advantages of our proposed method, moreover, the proposed resource block design was very useful for facilitating the performance analysis and reducing the system costs.

References

[1] J. G. Apostolopoulos, P. A. Chou, B. Culbertson, T. Kalker, M. D. Trott, and S. Wee, "The road to immersive communication," *Proc. IEEE*, vol. 100, no. 4, pp. 974–990, April 2012.

[2] M. Hu, L. Wang, B. Tan, and S. Jin, "Two-tier 360-degree video delivery control in multiuser immersive communications systems," *IEEE Trans. Veh. Technol.*, vol. 72, no. 3, pp. 4119–4123, Mar. 2023.

[3] A. A. Zaidi, R. Baldemair, V. Moles-Cases, N. He, K. Werner, and A. Cedergren, "OFDM numerology design for 5G new radio to support IoT, eMBB, and MBSFN," *IEEE Commun. Stand. Mag.*, vol. 2, no. 2, pp. 78–83, 2018.

[4] P. Guan, D. Wu, T. Tian, J. Zhou, X. Zhang, L. Gu, A. Benjebbour, M. Iwabuchi, and Y. Kishiyama, "5G field trials: OFDM-based waveforms and mixed numerologies," *IEEE J. Sel. Areas Commun.*, vol. 35, no. 6, pp. 1234–1243, June 2017.

[5] L. You, Q. Liao, N. Pappas, and D. Yuan, "Resource optimization with flexible numerology and frame structure for heterogeneous services," *IEEE Commun. Lett.*, vol. 22, no. 12, pp. 2579–2582, Dec 2018.

[6] X. Zhang, L. Zhang, P. Xiao, D. Ma, J. Wei, and Y. Xin, "Mixed numerologies interference analysis and inter-numerology interference cancellation for windowed OFDM systems," *IEEE Trans. Veh. Technol.*, vol. 67, no. 8, pp. 7047–7061, Aug. 2018.

[7] E. Memisoglu, A. E. Duranay, and H. Arslan, "Numerology scheduling for PAPR reduction in mixed numerologies," *IEEE Wireless Commun. Lett.*, vol. 10, no. 6, pp. 1197–1201, June 2021.

[8] K. Boutiba, M. Bagaa, and A. Ksentini, "Radio resource management in multi-numerology 5G new radio featuring network slicing," in *Proc. IEEE ICC*, 2022, pp. 359–364.

[9] T.-S.-L. Nguyen, S. Kallel, N. Aitsaadi, C. Adjih, and I. Fajjari, "A flexible numerology configuration for efficient resource allocation in 3GPP V2X 5G new radio," in *IEEE GLOBECOM*, 2022, pp. 4449–4454.

[10] H. Yin, L. Zhang, and S. Roy, "Multiplexing URLLC traffic within eMBB services in 5G NR: Fair scheduling," *IEEE Trans. Commun.*, vol. 69, no. 2, pp. 1080–1093, Feb. 2021.

[11] M. Setayesh, S. Bahrami, and V. W. Wong, "Resource slicing for eMBB and URLLC services in radio access network using hierarchical deep learning," *IEEE Trans. Wireless Commun.*, vol. 21, no. 11, pp. 8950–8966, Nov. 2022.

[12] M. Darabi, V. Jamali, L. Lampe, and R. Schober, "Hybrid puncturing and superposition scheme for joint scheduling of URLLC and eMBB traffic," *IEEE Commun. Lett.*, vol. 26, no. 5, pp. 1081–1085, May 2022.

[13] L. Marijanović, S. Schwarz, and M. Rupp, "Multiplexing services in 5G and beyond: Optimal resource allocation based on mixed numerology and mini-slots," *IEEE Access*, vol. 8, pp. 209 537–209 555, Nov. 2020.

[14] A. Yaqoob, T. Bi, and G.-M. Muntean, "A survey on adaptive 360° video streaming: Solutions, challenges and opportunities," *IEEE Commun. Surv. Tutor.*, vol. 22, no. 4, pp. 2801–2838, 2020.

[15] L. Sun, F. Duanmu, Y. Liu, Y. Wang, Y. Ye, H. Shi, and D. Dai, "A two-tier system for on-demand streaming of 360 degree video over dynamic networks," *IEEE J. Emerg. Sel. Topics Circuits Syst.*, vol. 9, no. 1, pp. 43–57, July 2019.

[16] T. C. Nguyen and J.-H. Yun, "Predictive tile selection for 360-degree VR video streaming in bandwidth-limited networks," *IEEE Commun. Lett.*, vol. 22, no. 9, pp. 1858–1861, Sept. 2018.

[17] Y. Zhang, P. Zhao, K. Bian, Y. Liu, L. Song, and X. Li, "DRL360: 360-degree video streaming with deep reinforcement learning," in *Proc. IEEE INFOCOM*, 2019, pp. 1252–1260.

[18] N. Kan, J. Zou, C. Li, W. Dai, and H. Xiong, "Rapt360: Reinforcement learning-based rate adaptation for 360-degree video streaming with adaptive prediction and tiling," *IEEE Trans. Circuits Syst. Video Technol.*, vol. 32, no. 3, pp. 1607–1623, Mar. 2022.

[19] C. Guo, L. Zhao, Y. Cui, Z. Liu, and D. W. K. Ng, "Power-efficient wireless streaming of multi-quality tiled 360 VR video in MIMO-OFDMA systems," *IEEE Trans. Wireless Commun.*, vol. 20, no. 8, pp. 5408–5422, Aug. 2021.

[20] 3GPP TS 38.211, "NR; Physical channels and modulation (Release 17)," June 2023.

[21] F. Pardo, A. Tavakoli, V. Levdik, and P. Kormushev, "Time limits in reinforcement learning," in *Pro. ICML*, 2018, pp. 1–10.

[22] V. Mnih *et al.*, "Human-level control through deep reinforcement learning," *Nature*, vol. 518, no. 7540, pp. 529–533, Feb. 2015.

[23] S. Schwarz, C. Mehlführer, and M. Rupp, "Low complexity approximate maximum throughput scheduling for LTE," in *Asilomar Conf. Signals Syst. Comput.*, 2010, pp. 1563–1569.